GTP-18-1278

WALL TEMPERATURE MEASUREMENTS IN GAS TURBINE COMBUSTORS WITH THERMOGRAPHIC PHOSPHORS

Patrick Nau*, Zhiyao Yin, Oliver Lammel, Wolfgang Meier

Institute of Combustion Technology
German Aerospace Center (DLR)
70569 Stuttgart, Germany
Email: patrick.nau@dlr.de

ABSTRACT

Phosphor thermometry has been developed for wall temperature measurements in gas turbines and gas turbine model combustors. An array of phosphors has been examined in detail for spatially and temporally resolved surface temperature measurements. Two examples are provided, one at high pressure (8 bar) and high temperature and one at atmospheric pressure with high time resolution.

To study the feasibility of this technique for full scale gas turbine applications a high momentum confined jet combustor at 8 bar was used. Successful measurements up to 1700 K on a ceramic surface are shown with good accuracy. In the same combustor, temperatures on the combustor quartz walls were measured, which can be used as boundary conditions for numerical simulations.

An atmospheric swirl-stabilized flame was used to study transient temperature changes on the bluff body. For this purpose, a high-speed setup (1 kHz) was used to measure the wall temperatures at an operating condition where the flame switches between being attached (M-flame) and being lifted (V-flame) (bistable). The influence of a precessing vortex core (PVC) present during M-flame periods is identified on the bluff body tip, but not at positions further inside the nozzle.

NOMENCLATURE

Acronyms	
FFT	Fast Fourier Transformation
FLOX	Flameless oxidation
HBK-S	Optical high-pressure test rig of the DLR Institute of Combustion Technology
LIF	Laser Induced Fluorescence
LIP	Laser Induced Phosphorescence
PIV	Particle Image Velocimetry
PMT	Photomultiplier Tube
PVC	Precessing Vortex Core
TBC	Thermal Barrier Coating
UV	Ultraviolet
YAG	Yttrium Aluminum Garnet
Symbols	
A	Amplitude of exponential decay curve
f	Focal length
$I(t)$	Intensity of signal at time t
o	Offset
T	Temperature
t	Time
t_{start}, t_{end}	Start and end time of the fitting window
x, y, z	Burner coordinates
λ	Air excess ratio
σ	Standard deviation
τ	Phosphorescence decay rate

*Address all correspondence to this author.

INTRODUCTION

The wall temperatures of gas turbine combustors play an important role in the performance of gas turbines. In order to protect the wall material from excessive temperatures, cooling air is needed. However, this reduces the efficiency of the gas turbine and can cause higher CO emissions due to the presence of cold zones near the walls. An exact knowledge of the wall temperature is important to determine an optimal cooling air flow. Furthermore, numerical simulations are generally applied for the development of gas turbines. To evaluate and improve the reliability of numerical predictions, comprehensive data sets are needed in technically-relevant flames under elevated pressures with well-defined boundary conditions. An important parameter in this respect is the temperature of the combustor wall. Increasing attention has been drawn in recent years to heat loss to the confinement and the influence on flame stabilization. Due to the lack of accurate measurements, this is often neglected in numerical simulations e.g. with assumed adiabatic walls.

Various wall temperature measurement techniques exist. Online techniques (like thermocouples, or pyrometry) can provide time-resolved temperatures, while offline techniques (like thermal paints) can only provide the maximum temperature during the experiment. Thermocouples are widely used, well understood and can provide temperatures with high accuracy. Because a thermocouple requires direct contact to the component of interest, it is intrusive, which is the main drawback of the technique. Furthermore only point measurements are possible and the wiring can be difficult.

Pyrometry offers several advantages compared to thermocouples. It uses the thermal radiation emitted from the sample to obtain the temperature and is therefore non-intrusive. A high temporal and spatial resolution of the measured temperature is possible. However the technique can suffer from flame emissions and reflected radiation in combustors [1, 2]. These effects can limit the accuracy in gas turbine applications.

A widely applied offline measurement technique is thermal indicating paint. These paints undergo an irreversible color change, when heated above a certain temperature. The color change is interpreted after testing and isotherms at the color change temperature are obtained [3]. Other techniques use the physical change of a material due to heat treatment. Thermal crystals are irradiated before the experiment and later analysed with X-ray diffraction to obtain the temperature [4]. Thermal history paints rely on ceramic materials doped with luminescent transition or rare-earth ions [5]. The luminescent lifetime changes irreversibly, when treated with high temperatures. This change in lifetime is measured precisely after testing. One of the advantages of offline techniques is that they do not require optical access to the surface of interest during testing. As a main drawback only the maximum temperature during testing is obtained. Therefore a large number on individual tests may be needed.

As an alternative, surface thermometry with laser-induced phosphorescence (LIP) employing temperature-sensitive phosphorescent particles can provide precise temperature measurements with high spatial and temporal resolution [6–9]. For this purpose, the surface is coated with a thin phosphorescent layer, similar to thermal history paints. However, the change in luminescent lifetime is reversible and therefore the temperature is measured online. The phosphorescent particles usually consist of a ceramic host doped with transition or rare earth metals. After excitation by a light source (mostly ultraviolet (UV), preferably a short pulse laser), these materials emit light after several internal energy transfer processes. At high temperatures the non-radiative quenching reduces the lifetime of the phosphorescence. Because of the resulting temperature dependence of the lifetime, this approach is often used to obtain the temperature from the temporal decay of the phosphorescence. The temperature dependence of the thermal quenching depends on the actual energy levels and is therefore material specific. It can often be described by an exponential dependence on the energy gap [10, 11]. Alternatively to the decay rate method, the intensity ratio of two emission lines can be used for some phosphors to determine the temperature [12]. This approach is generally much less sensitive [13].

One phosphor is typically sensitive in a range of about 300–400 K. Moreover, the decay rate of the phosphor at the temperature of interest must be considered, when high temporal resolution is required [14]. Some applications in gas turbines have already been reported. Examples include temperatures on stator vanes [15, 16] or on rotating turbine blades [17].

Critical aspects of the technique for measurements in gas turbines are the maximum temperature range and high temporal resolution, to capture transient changes or for measurements on moving objects. In this work we want to address both aspects. For applications in a full scale gas turbine, or a gas turbine model combustor, wall temperatures cover a few hundred Kelvin up to almost 2000 K. For this broad temperature range several phosphors have to be used. We will present results from five phosphors (Al_2O_3:Cr (ruby), YAG:Dy, YAG:Eu, YAG:Tb and Mg_4FGeO_6:Mn) and discuss their sensitivity and reliability. These phosphors will allow wall temperature measurements from room temperature up to 1800 K. Two applications will be shown to demonstrate wall temperature measurements at high temperatures (up to 1800 K) and pressures (8 bar), and with high temporal resolution (1 kHz) using a high-speed laser and camera system. While conditions in the high pressure combustor are close to conditions in a full scale gas turbine, an atmospheric pressure combustor was used to demonstrate the high-speed capabilities of the technique for capturing transient wall temperature changes.

EXPERIMENTAL SETUPS AND DATA EVALUATION

Depending on the experiment, different optical setups were used. Phosphor samples were excited either with a Nd:YAG laser (532 nm, 355 nm or 266 nm) or a high-speed dye laser (283 nm), while phosphorescence signals were detected with a photomultiplier tube (PMT), a spectrometer or a high-speed camera.

Data evaluation

The phosphorescence signal can be described as an exponentially decaying curve

$$I(t) = o + A \cdot e^{-t/\tau} \tag{1}$$

with intensity I at time t, amplitude A, offset o and decay rate τ. The offset was substracted from the measurement data before further data analysis. For decay curves acquired with a PMT and oscilloscope the region of the time trace just before the decay curve was used to determine the offset o. For measurements with a camera the offset was determied from a background image with the laser beam blocked. The decay rate is determined with a nonlinear least-square fitting process. However, in reality the decay curve shows multi-exponential behavior. For a multi-exponential curve the number of free fitting parameters is very high, therefore it is not practical to fit this to the measured signal. Instead a mono-exponential model is combined with a carefully controlled fitting window. This is necessary, because for multi-exponential decays the determined decay rate depends on the section of the decay curve used for the data evaluation. One approach proposed by Brübach *et al.* [18] defines the start and end time (t_{start} and t_{end} respectively) of the fitting window based on the decay rate ($t_{\text{start}} = c_1 \times \tau$ and $t_{\text{end}} = c_2 \times \tau$). Therefore an iterative fitting process is needed to determine τ. This approach is useful for curves with pronounced multi-exponential behavior or in case of a short spike (e.g. from interfering fluorescence or laser scattering) at the beginning of the curve. Alternatively the fitting window is described as the time, when the intensity has dropped below a certain fraction of the initial amplitude A. This approach is for example often used for Cavity Ring-down Spectroscopy [19], but only useful for weak multi-exponential behavior.

Calibration and characterization

Before measuring temperatures with a thermographic phosphor, calibration measurements must be performed. For this purpose the sample (powder or coated surface) was placed inside a furnace (LAC, VP 10/16, Boldt Wärmetechnik GmbH) and a reference thermocouple (type B or type K) was placed as close as possible to the sample. The decay rate of the phosphorescence was then measured at different temperatures. Excitation and detection setup and data evaluation procedures were kept as close as possible to the conditions during the actual temperature measurements to avoid systematic errors.

In addition to decay rate measurements, emission spectra of the phosphors were measured. For these measurements the phosphor sample was placed inside a furnace to perform measurements at elevated temperatures. Spectra at high temperatures were captured with an echelle spectrograph (ESA 4000EV/i, LLA Instruments GmbH) equipped with an intensified camera. Gating of the camera helps to suppress the thermal background at high temperatures. Room temperature spectra were captured with a Czerny-Turner spectrometer (AvaSpec-2048-USB2, Avantes).

Phosphor coating

Phosphor coatings were applied with a mixture of a commercial binder (Zyp coatings) with the phosphor powder (Al_2O_3:Cr, YAG:Dy and YAG:Eu from Phosphor Technology, YAG:Tb from Leuchtstoffwerk GmbH and SV67 from Osram GmbH). A mixing ratio of 0.1 g phosphor powder to 1 mL binder was used. The mixture was spray painted onto the surface with an air brush (Badger 100). To increase homogeneity of the coating, several layers were painted on the window and dried with a heat gun after each layer. After that, the substrates were heated in a furnace at 350 °C for 1 h and 1000 °C for 1 h. The layer thickness was controlled with a coating thickness gauge (Sauter, TE 1250-0.1FN) to achieve a thickness of about 20 µm. In previous studies [20] no temperature gradient could be found for a thickness below 20 µm, and therefore only a minor influence of the coating on the heat flux is expected. The homogeneity of the coating was measured with the coating thickness gauge at 3–5 positions and inspected visually.

Several commercial binders (Zyp coatings) were qualitatively tested to determine a binder that gives best durability at high temperatures and easy handling. For this purpose the binder mixture was spray painted on several substrates, heated to a given temperature and the coating visually inspected after cooling down to room temperature. The results are summarized in Tab. 1. The tested substrates include a polished quartz plate, a stainless steel plate, a magnesia substrate and a piece of thermal barrier coating (TBC). The TBC is an yttrium stabilized zirconia that had been plasma sprayed onto a steel substrate. A piece of the coated substrate was treated with aqua regia (hydrochloric and nitric acid, ratio 1:3) for several hours until the coating separated from the steel substrate. The TBC coating was then tested in the high temperature furnace without the metal substrate. HPC binder performed best for coatings on quartz and steel, while on ceramic substrates LRC gives the best results. Both binders are water based and therefore easy to apply and not toxic.

binder	tested substrate and temperature				
	quartz	steel	MgO	MgO	TBC
	1300 K	1300 K	1300 K	1700 K	1700 K
Gel-P	–	–	+	–	
HPC	+	+	+	+	o
LRC	o	o	+	+	+
BNSL	o	–	–	–	
ZAP	+	–	o	–	

TABLE 1. **Qualitative results for the durability of the coating using commercial binders from Zyp coatings. + = good (no degradation visible), o = medium (coating degradation visible, but still more than about 50 % left), - = bad (coating almost completely gone).**

High-speed measurements

High-speed measurements were performed in an atmospheric pressure model combustor. The combustor used in this work has already been studied in several investigations [21, 22]. For details we refer to the literature and will only give a brief description here. A schematic of the setup is shown in Fig. 1. A mixture of methane and air (air excess ratio $\lambda = 1.43$, thermal load 20 kW) was delivered into a cylindrical plenum (78 mm diameter), passed a swirl generator with 12 vanes and entered the combustor via a converging nozzle (27.85 mm diameter) with a central conical bluff body. The combustor had a square cross section of 85×85 mm^2, is 114 mm long, with an exhaust duct of 40 mm diameter. All four walls of the combustor were equipped with quartz windows to allow optical access. The operating condition discussed here was recently investigated by Yin et al. [23].

For excitation of the phosphor a commercial high-speed dye laser system (Cobra-Stretch HRR, Sirah GmbH) pumped by the second harmonic output of a diode-pumped solid state Nd:YLF laser (IS-811E, Edgewave) was used. The dye laser was frequency doubled and tuned to 283.2 nm (1 kHz, 50 µJ pulse energy). This wavelength allowed convenient excitation of OH radicals in the flame as well as the phosphor coating (SV67 used here, see Tab. 2). The laser beam was expanded to a sheet with two cylindrical lenses (f_1 = -50 mm and f_2 = 250 mm) and then softly focused waist-wise with a f_3 = 1000 mm cylindrical lens. The laser sheet passed the center of the combustion chamber for OH laser induced fluorescence (LIF) measurements and was then directed with a periscope back onto the base plate and the bluff body of the combustor for simultaneous phosphorescence measurements. The base plate and bluff body were coated with a 4×80 mm^2 wide strip of SV67 using the HPC binder (Zyp coatings). This way a 80 mm line of the phosphor coating could be excited.

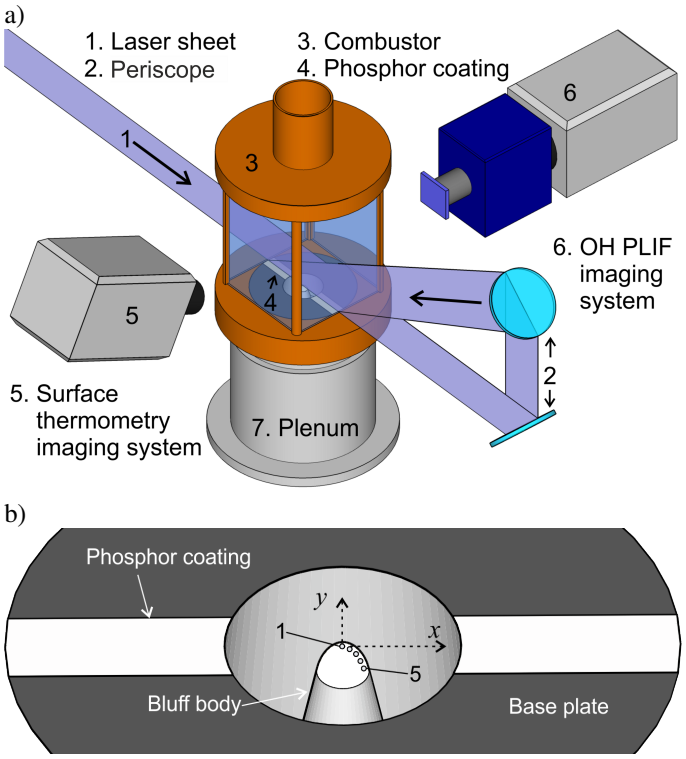

FIGURE 1. **a) Schematic of the optical setup for simultaneous phosphor thermometry and OH LIF measurements [23]. b) Phosphor coating on the base plate and bluff body of the combustor. Measurement positions 1–5 on the bluff body are marked.**

Phosphorescence was collected by a CMOS camera (LaVision HSS8, active sensor size 960×40 pixels) equipped with a lens (f = 85 mm, f/1.4, Canon). The angle between burner surface and camera was about 60°. No additional interference filter was used since the lens is not transmissive to the wavelength of the UV beam. The viewing angle of the camera and the angle of the excitation laser sheet allowed measurements on the bluff body at $y < 0$ mm. Decay rates were evaluated for five positions on the bluff body. Position 1 is the tip of the bluff body at $y = 0$ mm and position 5 is at about $y = -2$ mm (see Fig. 1b).

The camera was triggered at 70 kHz with a gate width of about 14 µs, resulting in 70 data points for each decay trace. A software binning of 7×7 pixels was used to smooth the signal, resulting in a spatial resolution of 0.8×0.8 mm^2. A background image was obtained prior to each set of measurements by blocking the laser beam. This background was subtracted from each image. An exponential curve (Eq. 1) was fitted to the decay curve between 90 % and 5 % of the peak intensity. Due to the used frame rate of the camera (70 kHz) the minimum measurable phosphorescence decay rate was limited to about 50 µs.

High pressure premixed jet flames

The experiments were carried out at the high pressure test rig HBK-S at DLR Stuttgart. Because the FLOX®combustor used here has been discussed in detail in previous publications, only a brief desciption is given here [24, 25]. This burner was designed to provide a fuel-flexible combustor (gaseous and liquid fuels) to gain deeper insight into jet stabilized flames with or without a pilot flame. The combustion chamber has a square cross section of $95 \times 95\,\mathrm{mm}^2$ and a length of 843 mm. Optical access was accomplished from all four sides with quartz window segments of $160 \times 90\,\mathrm{mm}^2$. The coordinate system is shown in Fig. 2. The origin is located at the burner base plate $x = 0$ mm and centered for y and z within the combustor chamber. The main nozzle with a diameter of 40 mm was off-centered by 10 mm and located at $z = 0$ mm and $y = -10$ mm. The operating conditions investigated here had a pressure of 8 bar, a preheat temperature of 725 K and a jet velocity of 111 m/s. Premixed natural gas/air flames with air excess ratios λ between 1.9 – 3.1 were investigated. The pilot flame was not used in this investigation.

A Nd:YAG laser (Spitlight 600, Innolas GmbH, 15 Hz repetition rate, 6 ns pulse length) was used for excitation of the phosphors. Depending on the phosphor an excitation wavelength of 266, 355 or 532 nm was used (see Tab. 2). An aperture (1.5 mm diameter) reduced the size of the laser beam. Depending on the phosphor and signal level laser energies between 0.3 and 3 mJ were used. A lens ($f = 100$ mm) focused the phosphorescence light onto a pinhole (diameter 300 µm) to reduce the detection volume and the collection of unwanted light. The light was collimated with a second lens and passed several filters depending on the phosphor. Typically a long pass filter (GG400, cut-off wavelength 400 nm for UV excitation) was used to remove stray light from the laser and a band pass filter with a bandwidth of 10 nm centered on the emission line of the phosphor (see Tab. 2). Transmitted light was then detected with a photomultiplier tube (PMT) (Hamamatsu R3896). PMT signals were captured with an oscilloscope (Agilent Technologies DSO7034B, 350 MHz) and transferred to a computer running a LabVIEW program for online signal processing and data storage.

Temperatures on the quartz walls were measured for case U described in Severin et al. [25] ($\lambda = 1.83$) and complement existing measurements from particle image velocimetry (PIV) and OH laser induced fluorescence (LIF). The phosphor (YAG:Eu and YAG:Dy) was coated at several positions as $4 \times 4\,\mathrm{mm}^2$ square points using the HPC binder. For excitation of these measurement points the laser beam and detection optics were moved with a stepper motor. Laser and detection optics were located at the same side of the window at a small angle. Excitation was accomplished from the back of the coating, therefore laser beam and phosphorescence signal did not have to pass through the flame (see Fig. 2). This way influences from beam steering were avoided.

A cylindrical alumina probe (diameter 20 mm, 40 mm tall) was placed in the exhaust region of the flame at $x = 680$ mm and $z = 0$ mm (see Fig. 2). The measurement position was at $y = -14$ mm, which means 33 mm from the combustor wall. A phosphor (YAG:Dy) coating was applied on the surface of the alumina probe.

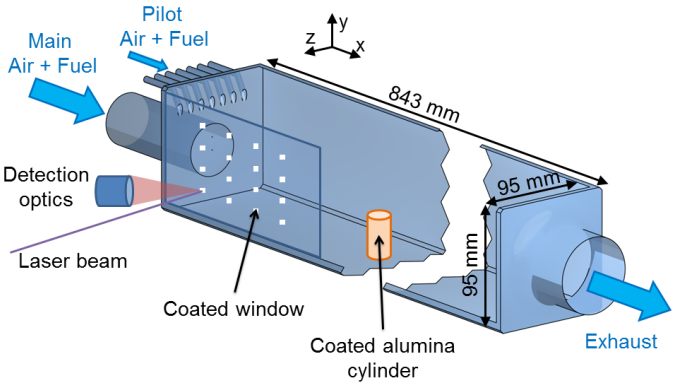

FIGURE 2. Schematic of the FLOX®model combustor with coordinate system, dimensions and optical arrangement for wall temperature measurements.

PHOSPHOR SELECTION AND CHARACTERIZATION

For characterization and testing of different phosphors, measurements in a furnace were performed. Overall five different types of phosphors were tested to cover temperatures from room temperature up to 1800 K. Table 2 gives an overview over the investigated phosphors, their excitation and detection wavelengths and the usable temperature ranges.

Emission spectra

Figure 3 shows emission spectra of all investigated phosphors. Spectra of YAG:Dy and YAG:Tb were measured at 1100 K, while the spectra of YAG:Eu [26], Al_2O_3:Cr (ruby) and Mg_4FGeO_6:Mn (SV67) were measured at room temperature. The detection wavelengths listed in Tab. 2 allow minimal overlap of the emission spectra. In addition, the excitation wavelength can be changed to further minimize the cross talk. Therefore it is possible to mix different phosphors to extend the temperature range that can be measured with a single coating. It should be noted that, for YAG:Dy and SV67 it is possible to use the ratio of two emission lines to measure the temperature as well. However, because this approach is less sensitive (by about one order of magnitude), it was not used in this investigation [13].

TABLE 2. Excitation- and emission wavelengths and accessible temperature range of the investigated phosphors.

phosphor	excitation [nm]	detection [nm]	range [K]	comment
YAG:Dy	355	458	1400–1800	intensity ratio approach possible at T< 1450 K
YAG:Eu	266	614	1000–1600	influence from reducing atmospheres ($\sim$ 25 K)
YAG:Tb	266	543	1000–1450	multi-exponential; influence from substrate
Mg_4FGeO_6:Mn (SV67)	266 / 283 / 355	656	300–1050	broad temperature range
Al_2O_3:Cr (ruby)	532	694	300–800	only for low temperatures

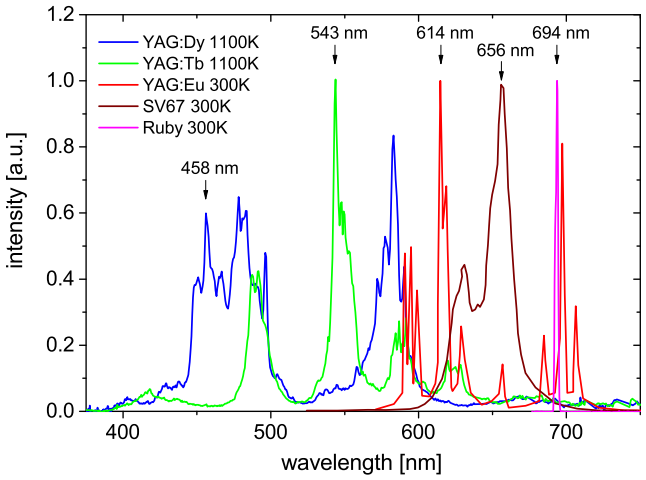

FIGURE 3. Emission spectra of the investigated phosphors after excitation at 355 nm (YAG:Dy and SV67), 266 nm (YAG:Eu and YAG:Tb) or 532 nm (ruby). Spectra of YAG:Dy and YAG:Tb were measured in a furnace at 1100 K. The spectrum of YAG:Eu is adapted from Kissel *at al.* [26] and measured at room temperature, as well as the spectra of SV67 and ruby.

Calibration and uncertainty analysis

The calibration curves (decay rate τ against temperature T) for these phosphors are shown in Fig. 4. All curves have been measured with the low speed laser setup and a PMT for detection. Calibration measurements obtained using the high-speed camera setup have been omitted for simplicity since they are consistent with the ones shown here. A polynomial is fitted to this curve to allow convenient calculation of the temperature from the measured decay rate in the experiment. From the calibration curves a sensitivity factor k is calculated:

$$k = \left| \frac{d\tau/\tau}{dT/T} \right| \qquad (2)$$

which is essentially the normalized first derivative of the calibration curve $\tau(T)$. It is computed from the polynomial fits to the calibration data shown in Fig. 4. The sensitivity factor allows a good visualization of the sensitive regions of the phosphor and estimation of the expected precision (Fig. 5). For example an error in the determined decay rate τ of 5 % at a sensitivity factor of 20 corresponds to an error in the temperature T of only 0.25 %.

The precision was determined from the standard deviation of individual laser shots at a constant temperature in the furnace. For the setup utilizing PMT and oscilloscope the precision is between 0.1–0.5 %. Due to the reduced number of data points of the decay curves obtained with the camera (70 compared to 1000) the precision is slightly lower in this case (0.5–0.9 %).

The measurement accuracy mainly depends on errors from the calibration procedure and is comparable for both setups (high-speed camera or PMT). This includes the accuracy of the reference thermocouple (0.25 %), a temperature gradient between thermocouple and sample inside the furnace (estimated to 0.2 %) and temperature stability inside the furnace ($\pm$ 1 K). This sums up to a maximum contribution to the error between 3 K at 400 K and 9 K at 1800 K or 0.5 – 0.75 %.

In addition, systematic errors can contribute to the uncertainty. The influence of the laser energy has been investigated for some phosphors before (for example SV67 [27], YAG:Dy and YAG:Eu [28] and $CdWO_4$ [29]). Considering pulse-to-pulse laser energy fluctuations of less than 10%, the contribution is well below 0.1 % and therefore of minor importance. Differences in the detection system (for example PMT and oscilloscope settings) can cause systematic errors of several Kelvin [29]. Furthermore the data evaluation procedure influences the obtained decay rate. Especially the selection of the fitting window can have a significant impact, as will be shown in the next section in Fig. 6, when comparing the phosphors YAG:Tb and YAG:Eu. Therefore, these settings were kept identical between calibration and experiment to avoid systematic errors.

Discussion of different phosphors

Mg_4FGeO_6:Mn has already been used in various experiments (see [9] and references therein). It is sold as SV67 from

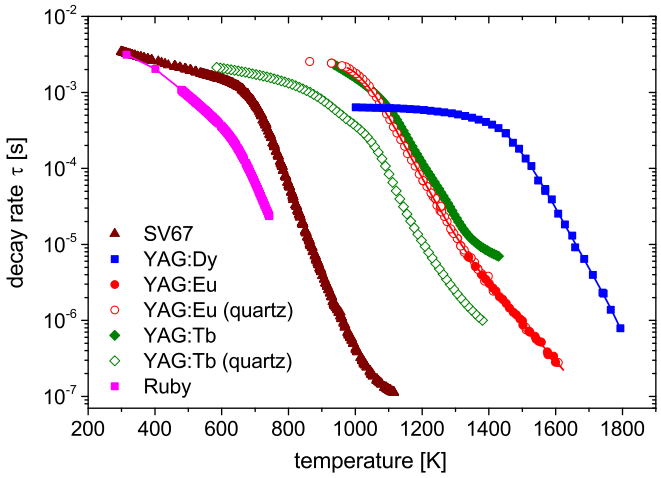

FIGURE 4. **Calibration curves for the investigated phosphors. A polynomial fitted to the measured data points is drawn as a line.**

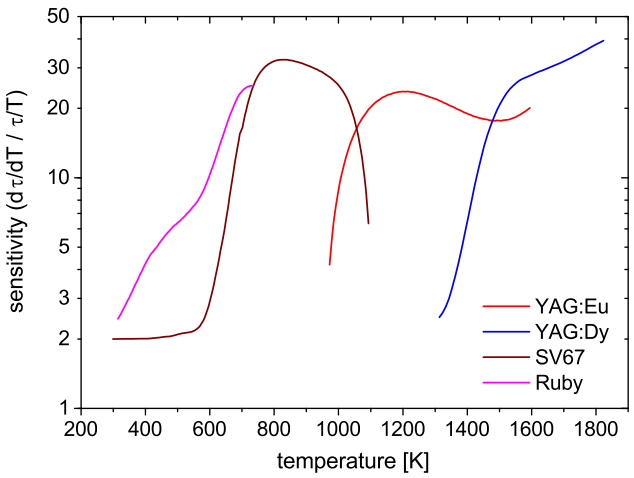

FIGURE 5. **Sensitivity of the investigated phosphors calculated with Eq. 2 from the calibration curves (decay rate τ against temperature T) shown in Fig. 4.**

Osram GmbH and named SV67 hereinafter for simplicity. This phosphor shows no influence from gas composition or absolute pressure and can therefore provide reliable temperature measurements [27,30]. The calibration curve shows two temperature sensitive regions. A region with low sensitivity at low temperatures (300–650 K) and a region with high sensitivity at temperatures above 650 K. This makes it possible to measure a very broad temperature range with a single phosphor. The sensitivity, and therefore precision, is about a factor of 10 lower in the low temperature (<650 K) region (Fig. 5).

Al_2O_3:Cr (ruby) is an alternative to SV67 for temperatures below 650 K. The sensitivity is higher than for SV67 in this region. This phosphor shows strong emission as a sharp peak at 694 nm and can be excited at 532 nm.

For high temperatures yttrium aluminum garnet $Y_3Al_5O_{12}$ (YAG) is a well suited host material because of its high melting point (about 2220 K). Many activators show higher temperature ranges of sensitivity in this host than in other host materials [7].

YAG:Tb and YAG:Eu were investigated for temperatures above 1000 K. Both phosphors cover a similar temperature range and were compared regarding emission wavelengths, multi-exponential decay characteristics and influences from substrate or gas composition. YAG:Tb seems to be a very good candidate due to its strong emission at 543 nm. The green emission reduces influences from thermal radiation compared to phosphors emitting in the red (i.e. YAG:Eu at 614 nm). However, the decay curve of this phosphor shows a strong multi-exponential behavior (Fig. 6). The inset in Fig. 6 shows the determined decay rate depending on the fitting window using the fitting approach of Brübach et al. [18]. While for YAG:Tb the influence is very strong, for YAG:Eu, which has a similar decay rate at 1100 K, only a weak influence is visible. Possible systematic errors are therefore much lower for YAG:Eu. In addition, the choice of substrate influences the measured decay rate for YAG:Tb, while no influence is found for YAG:Eu (see Fig. 4). The calibration curve of YAG:Tb for a coating on quartz differs significantly from the powder sample. Such behavior has already been observed for other phosphors and substrates [27, 31]. It was speculated that this might be caused by changes in the structure of the phosphor. Furthermore, fluorescence from the quartz substrate, which can occur at an excitation wavelength of 266 nm, might influence the phosphorescence measurements. However, it seems unlikely that the short fluorescence influences the decay measurement at long decay rates. Moreover, this effect was not observed for YAG:Eu, which is also excited at 266 nm. For YAG:Eu it has been reported that a reducing methane/nitrogen atmosphere will shift the calibration curve by about 25 K, probably due to redox reactions [26]. However, for a gas turbine application with typically lean conditions this should not cause systematic errors. Altogether YAG:Eu is a more reliable choice for temperatures above 1000 K. Using a sufficiently fast detection system temperatures up to 1600 K can be measured. At higher temperatures, however, thermal radiation becomes significant. At about 1300 K the thermal background is already as strong as the amplitude A of the decay curve, when using an excitation energy of 1 mJ. Averaging is therefore necessary to improve the signal-to-noise ratio and avoid errors from fluctuating background. Therefore a blue emitting phosphor is preferred.

YAG:Dy is a phosphor that can provide measurements at very high temperatures. Values up to 1970 K have been reported [32]. Typically emission lines at 490 nm or 458 nm are used, while the line at 458 nm is only populated at high temperatures. The emission line at 458 nm is preferred, due to the reduced in-

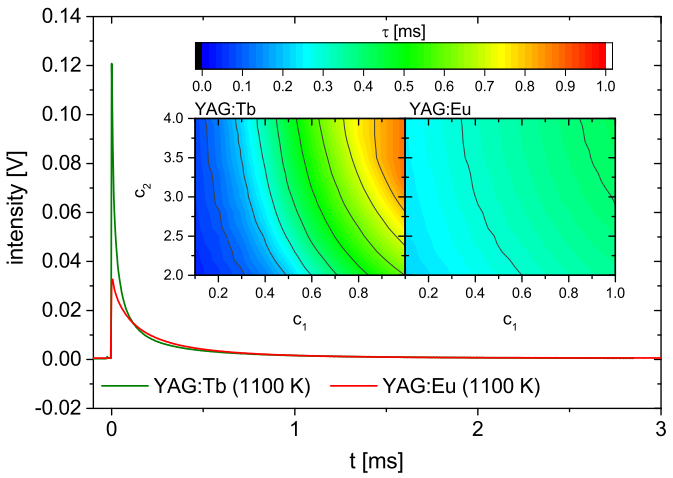

FIGURE 6. **Decay curves of YAG:Tb and YAG:Eu at 1100 K. The inset shows the influence of the fitting window ($t_{\mathbf{start}} = c_1 \times \tau$ and $t_{\mathbf{end}} = c_2 \times \tau$ as defined in [18]) on the obtained decay rate.**

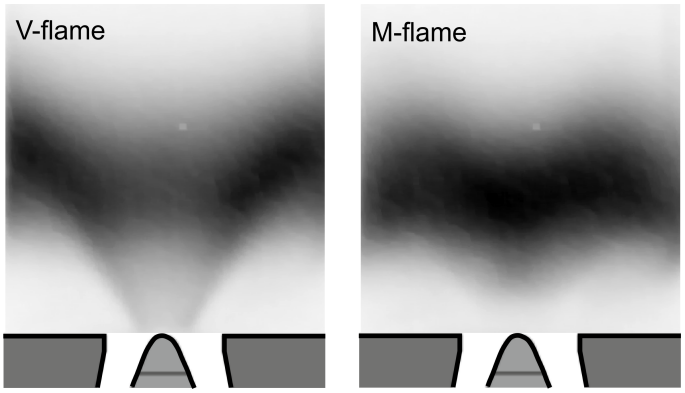

FIGURE 7. **Average OH* chemiluminescence images taken during the V- and M-flame periods adopted from Yin et al. [23].**

fluence from thermal radiation at this shorter wavelength. A doping level of 3 % has been reported to provide the highest signal levels [33]. Co-doping with a sensitizer like Er, Tm, Tb, Pr or BN has been investigated for this phosphor [33–35]. However, at least for Er co-doping (1.5 % Dy, 0.5 % Er) we found a pronounced multi-exponential behavior of the decay curve. Therefore we recommend using the not co-doped YAG:Dy phosphor, when the decay rate method is used.

RESULTS OF WALL TEMPERATURE MEASUREMENTS

In this section, the results from wall temperature measurements at high temperatures and pressures in confined jet flames and high-speed measurements at atmospheric pressure will be presented.

High-speed measurements at atmospheric pressure

Wall temperature measurements using a high-speed laser and camera setup were performed in an atmospheric swirl flame. The flame investigated here is bi-stable and randomly transitions between a lifted flame (M-shape) and a flame attached to the bluff body (V-shape). Average OH* chemiluminescence images during both periods are shown in Fig. 7 illustrating the V- and M-shaped flames [23]. The transition from an attached V-flame to a lifted M-flame occurs after a local extinction near the flame root and formation of a precessing vortex core (PVC), while the PVC is suppressed when the flame transitions back to the V-flame [36].

Periods of M- and V-flame were identified with simultaneous OH-LIF measurements [23]. Fig. 8 shows the temperature on the bluff body for a period of four seconds. The temperature increases up to a certain point during attached V-flame operation (white regions) and decreases when lifted (M-flame regions marked grey). During the attached flame periods (V-flame) the flame is close to the bluff body surface, which can explain the higher wall temperatures. While the change between M- and V-flame is very pronounced in the temperature on the bluff body tip (position 1) it becomes less obvious with increasing distance to the tip. During M-flame periods, the fluctuations of the temperature are quite strong. These fluctuations are strongest on the tip (position 1). While during M-flame periods the standard deviation of the temperature is about 17 K, it is only 10 K during V-flame periods. To investigate this further the time traces during M-flame operation were transferred into the frequency domain using a Fast Fourier Transformation (FFT). The resulting spectrum for the M-flame shows a peak at 475 Hz, while no peak is visible for the V-flame. This peak has an amplitude of about 7 K at position 1 ($y = 0$ mm), but becomes gradually smaller and finally completely vanishes for position 5 ($y = -2$ mm). The frequency matches very well to the PVC frequency of 490 Hz measured before for this condition with pressure transducers [37]. The results suggests that the larger temperature fluctuations on the bluff body during lifted M-flame periods can be attributed to the more dynamic environment and the presence of a PVC. Small discrepancies in the frequency reported in [37] and the one observed here might be attributed to slightly different operating conditions. The results clearly demonstrate the possibility to capture even fast temperature changes on the surface. The reduced influence of the PVC on the wall temperature for $y < 0$ mm gives additional information on the penetration of the PVC into the nozzle. PIV measurements have not been performed so far for $y < 0$ mm due to difficulties from laser scattering inside the nozzle. Therefore the origin and penetration of the PVC inside the nozzle remains an ongoing question [37].

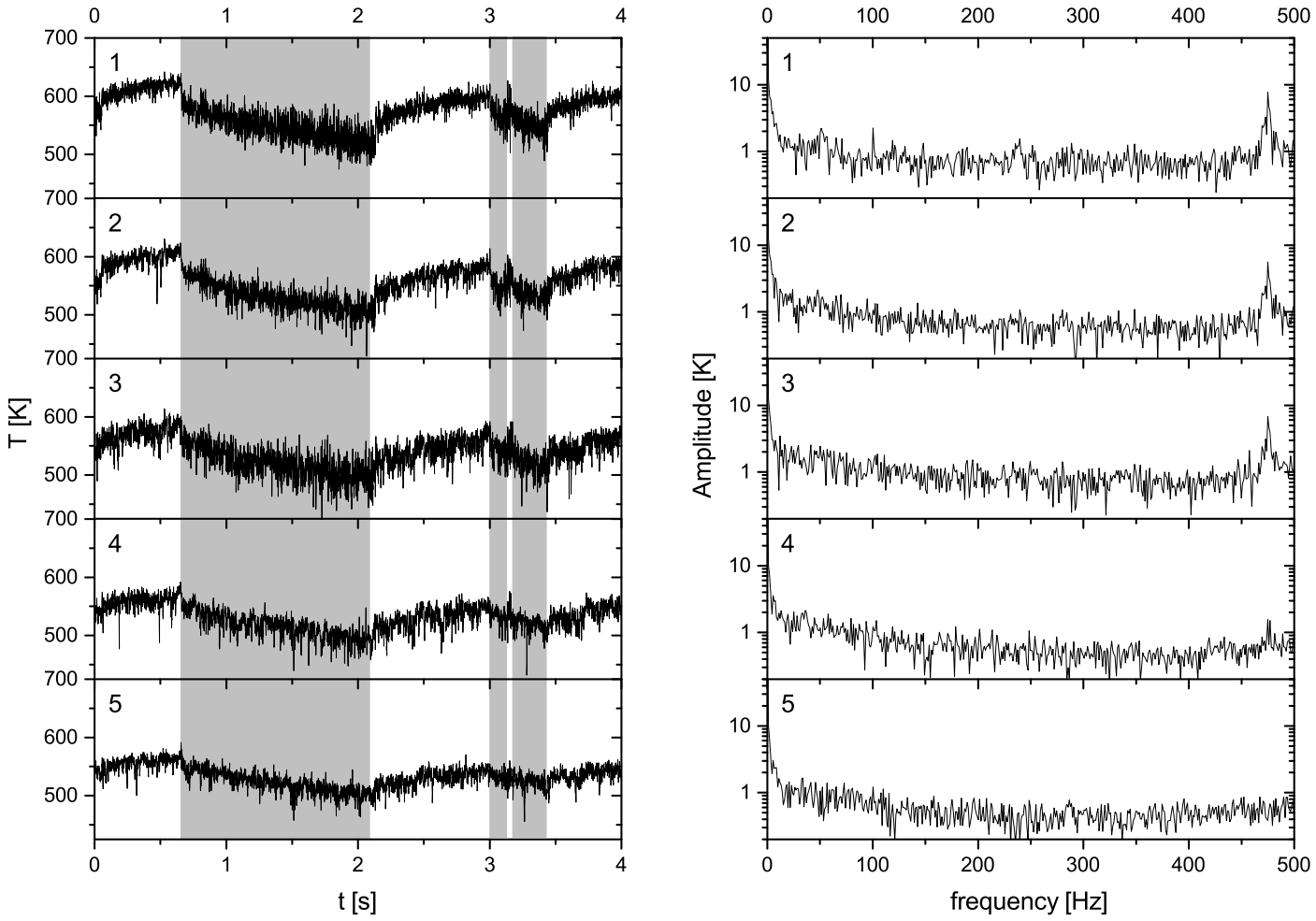

FIGURE 8. **Time traces of the wall temperature (left) on the bluff body for positions 1 (bluff body tip, $y = 0$ mm) to 5 ($y = -2$ mm). The gray regions in the time traces denote M-shape flame operation and were used for the calculation of the FFT (right).**

High pressure wall temperature measurements

To mimic the conditions of a TBC-coated gas turbine combustor wall, temperature measurements were carried out on the surface of a cylindrical alumina probe placed in the exhaust region of a jet stabilized enclosed natural gas flame at 8 bar. To achieve different temperatures on the probe, the air excess ratio λ of the flame was varied between 1.9 – 3.1. Starting at $\lambda = 2.2$ the stoichiometry was step wise changed to $\lambda = 2.55$, then λ was decreased up to 1.8 and then again increased up to 3.1. This way a possible hysteresis can be identified. In Fig. 9 the temperatures on the probe are plotted against the calculated adiabatic flame temperature using the program Gaseq [24, 38]. The relative standard deviation σ/T, determined from 150 individual laser shots, is plotted in the lower section. The wall temperature shows a linear dependence on the gas temperature and no hysteresis is visible. The relative standard deviation is below 0.5 % for all investigated conditions except for the two hottest conditions, were it is below 1 %. This shows the high precision and reliability of the method. The shot-to-shot standard deviation includes influences from laser energy fluctuations, the error of the decay rate fitting procedure and temperature fluctuations on the wall. The accuracy of the calibration procedure in this temperature region is about 0.5 %, as described in the section Phosphor Selection and Characterization. Therefore the total measurement uncertainty is 0.5–1.0 % (or 7–17 K).

In addition to the measurements on the ceramic cylinder, measurements on the combustor quartz walls were performed in this combustor. These measurements are in particular valuable parameters for improved boundary conditions of numerical simulations. In Fig. 10 the temperature field obtained using

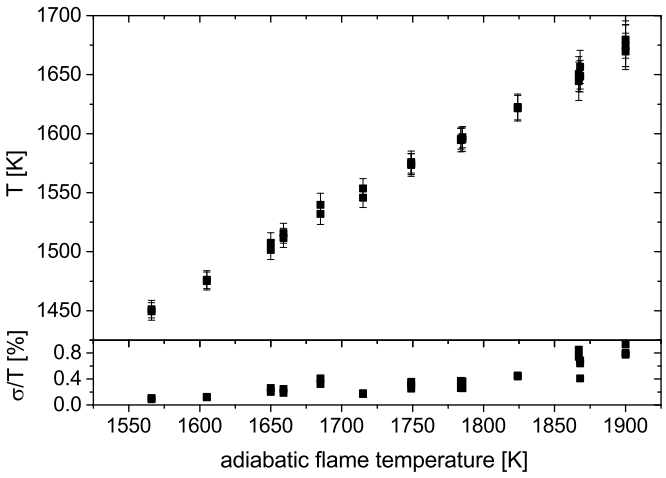

FIGURE 9. **Temperature on a ceramic probe for different flame conditions. Errors bars include errors from the calibration procedure and the measurement precision. The relative standard deviation of individual laser shots is shown in the bottom.**

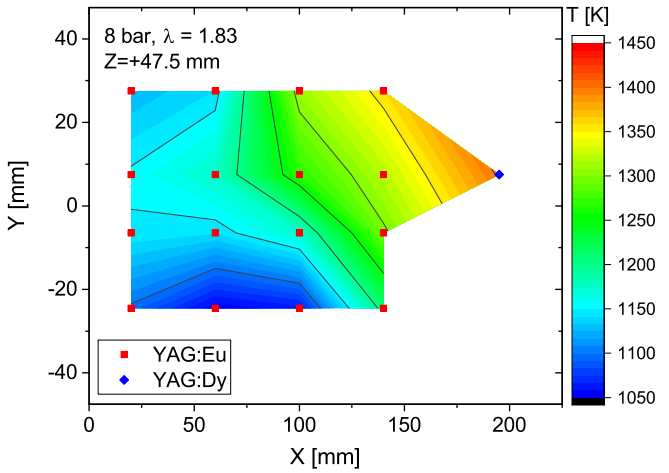

FIGURE 10. **Temperatures on the combustor quartz walls. The temperature field was interpolated between the measurement points (YAG:Eu: squares and YAG:Dy: diamonds).**

17 measurement positions is shown. Measured values are in the range of 1050–1400 K. Even higher values are expected further downstream and values below 1000 K are expected at larger absolute values of y. Temperatures increase along the x-axis and the maximum is slightly asymmetric along the y-axis due to the location of the main nozzle at $y = -10$ mm. The temperature field is in qualitative agreement with the flame location obtained from OH^* chemiluminescence and with gas temperatures obtained from OH-LIF measurements [24, 25].

Temperature measurements on the quartz walls were challenging for two reasons: Interfering fluorescence, probably from the quartz, and window degradation, especially for temperatures above 1400 K. It should be noted that these problems were not associated with the measurements on the ceramic probe mentioned above, where measurements up to 1700 K were possible. Window degradation results in the windows becoming opaque over time. In addition, the coating starts to degrade and therefore the signal level drops considerably. Interfering fluorescence was problematic in case of YAG:Eu. This phosphor is excited in the UV at 266 nm, in contrast to YAG:Dy which is excited at 355 nm, where fluorescence from quartz is unlikely. Similar problems have been reported before for phosphor thermometry in an optical engine [39]. Furthermore the decay rates of YAG:Eu are very short at high temperatures (about 1 µs at 1450 K), which makes it difficult to distinguish the already short phosphorescence from fluorescence (a few ns long). The short fluorescence (lifetime < 20 ns) causes a strong spike at the beginning of the phosphorescence decay curve. Therefore the phosphorescence curve is affected by the fluorescence due to excess photoelectrons in the PMT. This would result in apparently too short decay rates and therefore too high temperatures. The gain of the PMT must therefore be controlled carefully. This prevents using a higher gain at low signal levels. The measurement uncertainty on the quartz walls is therefore higher than on the ceramic probe (up to about 2 %). For measurements further downstream, a gated PMT could be used to remove the fluorescence spike from the beginning of the decay curve. This way a higher PMT gain could still be used in cases with low signal levels (e.g. due to window and coating degradation).

CONCLUSION

The capabilities of phosphor thermometry for wall temperature measurements in gas turbines and gas turbine model combustors were investigated. Several phosphors were tested and evaluated regarding sensitivity and reliability. A combination of three phosphors can be used to cover temperatures from room temperature up to 1800 K (Mg_4FGeO_6:Mn, YAG:Eu and YAG:Dy). These phosphors can be mixed in a single coating, when proper excitation and detection wavelengths are used. Coatings of combustor walls were accomplished with commercial chemical binders. Several binders were tested and the best binders identified for coatings on quartz glass, ceramic substrates and steel.

Successful wall temperature measurements were performed in two combustors: A swirl stabilized gas turbine model combustor at atmospheric pressure and a confined jet stabilized flame at 8 bar. These studies demonstrate temperature measurements at high temperatures and pressures and the possibility to resolve transient events in gas turbine combustors. Transient temperature changes were measured with a high-speed laser system (1 kHz)

in the atmospheric swirl flame. A bi-stable operating condition was chosen, where transitions between an attached V-flame and a lifted M-flame occur irregularly. The frequency of the PVC during M-flame periods is clearly visible in the frequency domain of the measured temperatures at 475 Hz, while it is not present during V-flame periods. By selecting a viewing angle from the top, it was possible to measure temperatures on the bluff body inside the nozzle. At larger distances from the nozzle exit ($y < 0$ mm) the peak in the frequency spectrum becomes smaller and finally disappears at $y = -2$ mm. These measurements might provide further insight into the formation and origin of the PVC.

Measurements at high pressure were performed to demonstrate the feasibility of the technique for applications in real gas turbines. A coated ceramic probe was used to mimic a TBC coated wall of a gas turbine combustor. Temperatures up to 1700 K were measured with high precision and accuracy. In addition, the wall temperatures of the combustor quartz walls were measured. These values can be used as boundary conditions for numerical simulations and complement existing optical measurements in this combustor.

ACKNOWLEDGMENT

The investigations were conducted as part of the joint research programs CEC (Siemens Clean Energy Center) and COOREFLEX-turbo in the frame of AG Turbo. The work was supported by the Bundesministerium für Wirtschaft und Energie (BMWi) as per resolution of the German Federal Parliament under Grant No. 03ET7011M, 03ET7073B, 03ET7011D and 03ET7020G. The authors gratefully acknowledge AG Turbo and Siemens AG Energy Sector for their support and permission to publish this paper. Zhiyao Yin acknowledges the financial support within the Helmholtz Postdoc Programme (Grant PD-112).

REFERENCES

[1] Kerr, C., and Ivey, P., 2002. "An overview of the measurement errors associated with gas turbine aeroengine pyrometer systems". *Meas. Sci. Technol.,* ***13***(6), pp. 873–881.

[2] Suarez, E., and Przirembel, H. R., 1990. "Pyrometry for turbine blade development". *J. Propul. Power,* ***6***(5), pp. 584–589.

[3] Lempereur, C., Andral, R., and Prudhomme, J. Y., 2008. "Surface temperature measurement on engine components by means of irreversible thermal coatings". *Meas. Sci. Technol.,* ***19***(10), p. 105501.

[4] Bachuchin, I. V., Zabusov, O. O., Morozov, V. A., Nikolaenko, V. A., and Saltykov, M. A., 2011. "Temperature measurement with irradiated materials". *At. Energy,* ***110***(3), pp. 178–183.

[5] Araguás Rodríguez, S., Jelínek, T., Michálek, J., Yáñez-González, Á., Schulte, F., Pilgrim, C. C., Feist, J. P., and Skinner, S. J., 2017. "Accelerated thermal profiling of gas turbine components using luminescent thermal history paints". In Proceedings of the 1st Global Power and Propulsion Forum, GPPF 2017.

[6] Allison, S. W., and Gillies, G. T., 1997. "Remote thermometry with thermographic phosphors: Instrumentation and applications". *Rev. Sci. Instrum.,* ***68***(7), pp. 2615–2650.

[7] Chambers, M., and Clarke, D., 2009. "Doped oxides for high-temperature luminescence and lifetime thermometry". *Annu. Rev. Mater. Res.,* ***39***(1), pp. 325–359.

[8] Aldén, M., Omrane, A., Richter, M., and Särner, G., 2011. "Thermographic phosphors for thermometry: A survey of combustion applications". *Prog. Energ. Comb. Sci.,* ***37***(4), pp. 422–461.

[9] Brübach, J., Pflitsch, C., Dreizler, A., and Atakan, B., 2013. "On surface temperature measurements with thermographic phosphors: A review". *Prog. Energ. Comb. Sci.,* ***39***(1), pp. 37–60.

[10] Dorenbos, P., 2005. "Thermal quenching of Eu^{2+} 5d-4f luminescence in inorganic compounds". *J. Phys.: Condens. Matter,* ***17***(50), p. 8103.

[11] Witkowski, D., and Rothamer, D. A., 2017. "A methodology for identifying thermographic phosphors suitable for high-temperature gas thermometry: application to Ce^{3+} and Pr^{3+} doped oxide hosts". *Appl. Phys. B,* ***123***(8), p. 226.

[12] Heyes, A., Seefeldt, S., and Feist, J., 2006. "Two-colour phosphor thermometry for surface temperature measurement". *Opt. Laser Technol.,* ***38***(46), pp. 257–265.

[13] Fuhrmann, N., Brübach, J., and Dreizler, A., 2013. "Phosphor thermometry: A comparison of the luminescence lifetime and the intensity ratio approach". *Proc. Combust. Inst.,* ***34***(2), pp. 3611–3618.

[14] Khalid, A. H., Kontis, K., and Behtash, H.-Z., 2010. "Phosphor thermometry in gas turbines: Consideration factors". *Proceedings of the Institution of Mechanical Engineers, Part G: Journal of Aerospace Engineering,* ***224***(7), pp. 745–755.

[15] Noel, B. W., Borella, H. M., Lewis, W., Turley, W. D., Beshears, D. L., Capps, G. J., Cates, M. R., Muhs, J. D., and Tobin, K. W., 1991. "Evaluating thermographic phosphors in an operating turbine engine". *J. Eng. Gas Turbines Power,* ***113***(2), pp. 242–245.

[16] Eldridge, J. I., Allison, S. W., Jenkins, T. P., Gollub, S. L., Hall, C. A., and Walker, D. G., 2016. "Surface temperature measurements from a stator vane doublet in a turbine afterburner flame using a YAG:Tm thermographic phosphor". *Meas. Sci. Technol.,* ***27***(12), p. 125205.

[17] Feist, J. P., Sollazzo, P. Y., Berthier, S., Charnley, B., and Wells, J., 2012. "Application of an industrial sensor coating system on a rolls-royce jet engine for temperature detection". *J. Eng. Gas Turbines Power,* ***135***(1), p. 012101.

[18] Brübach, J., Janicka, J., and Dreizler, A., 2009. "An algorithm for the characterisation of multi-exponential decay curves". *Opt. Lasers Eng.,* ***47***(1), pp. 75–79.

[19] Yalin, A. P., and Zare, R. N., 2002. "Effect of laser lineshape on the quantitative analysis of cavity ring-down signals". *Laser Phys.,* ***12***(8), p. 1065.

[20] Knappe, C., Algotsson, M., Andersson, P., Richter, M., Tunér, M., Johansson, B., and Aldén, M., 2013. "Thickness dependent variations in surface phosphor thermometry during transient combustion in an HCCI engine". *Combust. Flame,* ***160***(8), pp. 1466–1475.

[21] Steinberg, A., Arndt, C., and Meier, W., 2013. "Parametric study of vortex structures and their dynamics in swirl-stabilized combustion". *Proc. Combust. Inst.,* ***34***(2), pp. 3117–3125.

[22] Meier, W., Weigand, P., Duan, X., and Giezendanner-Thoben, R., 2007. "Detailed characterization of the dynamics of thermoacoustic pulsations in a lean premixed swirl flame". *Combust. Flame,* ***150***(1), pp. 2–26.

[23] Yin, Z., Nau, P., and Meier, W., 2017. "Responses of combustor surface temperature to flame shape transitions in a turbulent bi-stable swirl flame". *Exp. Therm Fluid Sci.,* ***82***, pp. 50–57.

[24] Lammel, O., Severin, M., Ax, H., Lückerath, R., Tomasello, A., Emmi, Y., Noll, B., Aigner, M., and Panek, L., 2017. "High momentum jet flames at elevated pressure, A: Experimental and numerical investigation for different fuels". In ASME Turbo Expo 2017. ASME Paper No. GT2017-64615.

[25] Severin, M., Lammel, O., Ax, H., Lückerath, R., Meier, W., Aigner, M., and Heinze, J., 2017. "High momentum jet flames at elevated pressure, B: Detailed investigation of flame stabilization with simultaneous PIV and OH-LIF". In ASME Turbo Expo 2017. ASME Paper No. GT2017-64556.

[26] Kissel, T., Brübach, J., Euler, M., Frotscher, M., Litterscheid, C., Albert, B., and Dreizler, A., 2013. "Phosphor thermometry: On the synthesis and characterisation of $Y_3Al_5O_12$:Eu (YAG:Eu) and $YAlO_3$:Eu (YAP:Eu)". *Mater. Chem. Phys.,* ***140***(2–3), pp. 435–440.

[27] Brübach, J., Feist, J. P., and Dreizler, A., 2008. "Characterization of manganese-activated magnesium fluorogermanate with regards to thermographic phosphor thermometry". *Meas. Sci. Technol.,* ***19***(2), p. 025602.

[28] Nau, P., Yin, Z., Geigle, K. P., and Meier, W., 2017. "Wall temperature measurements at elevated pressures and high temperatures in sooting flames in a gas turbine model combustor". *Appl. Phys. B,* ***123***(12), p. 279.

[29] Abou Nada, F., Knappe, C., Aldén, M., and Richter, M., 2016. "Improved measurement precision in decay time-based phosphor thermometry". *Appl. Phys. B,* ***122***(6), pp. 1–12.

[30] Brübach, J., Dreizler, A., and Janicka, J., 2007. "Gas compositional and pressure effects on thermographic phosphor thermometry". *Meas. Sci. Technol.,* ***18***(3), pp. 764–770.

[31] Pareja, J., Litterscheid, C., Kaiser, B., Euler, M., Fuhrmann, N., Albert, B., Molina, A., Ziegler, J., and Dreizler, A., 2014. "Surface thermometry in combustion diagnostics by sputtered thin films of thermographic phosphors". *Appl. Phys. B,* ***117***(1), pp. 85–93.

[32] Cates, M., Allison, S., Jaiswal, S., and Beshears, D., 2003. "YAG:Dy and YAG:Tm fluorescence to 1700 C". *Proc. Int. Instr. Symp.,* ***49***, pp. 389–400.

[33] Chepyga, L. M., Jovicic, G., Vetter, A., Osvet, A., Brabec, C. J., and Batentschuk, M., 2016. "Photoluminescence properties of thermographic phosphors YAG:Dy and YAG:Dy, Er doped with boron and nitrogen". *Appl. Phys. B,* ***122***(8), pp. 1–10.

[34] Jovicic, G., Zigan, L., Pfadler, S., and Leipertz, A., 2012. "Simultaneous two-dimensional temperature and velocity measurements in a gas flow applying thermographic phosphors". *16th Int Symp on Applications of Laser Techniques to Fluid Mechanics*, July 9–12.

[35] Hertle, E., Chepyga, L., Batentschuk, M., and Zigan, L., 2016. "Influence of codoping on the luminescence properties of YAG:Dy for high temperature phosphor thermometry". *J. Lumin.,* ***182***, pp. 200–207.

[36] Syred, N., 2006. "A review of oscillation mechanisms and the role of the precessing vortex core (PVC) in swirl combustion systems". *Prog. Energ. Comb. Sci.,* ***32***(2), pp. 93–161.

[37] Oberleithner, K., Stöhr, M., Im, S. H., Arndt, C. M., and Steinberg, A. M., 2015. "Formation and flame-induced suppression of the precessing vortex core in a swirl combustor: Experiments and linear stability analysis". *Combust. Flame,* ***162***(8), pp. 3100–3114.

[38] Morley, C. Gaseq, a chemical equilibrium program for windows. version 0.79b (accessed November 10, 2010). http://www.gaseq.co.uk/.

[39] Neal, N. J., Jordan, J., and Rothamer, D., 2013. "Simultaneous measurements of in-cylinder temperature and velocity distribution in a small-bore diesel engine using thermographic phosphors". *SAE Int. J. Engines,* ***6***(1), pp. 300–318.